MULTIFUNCTIONAL PERFORMANCE OF PVA-PVP/ZnO NANOCOMPOSITES: OPTICAL, DIELECTRIC AND AC CONDUCTIVITY ANALYSIS

T. Suma Chanu[1,3*], K. Jugeshwar Singh[2], and K. Nomita Devi[1]

[1]*Department of Physics, Manipur University, Canchipur, Imphal-795003, India*
[2]*Talent Development Centre, Indian Institute of Science, Kudapura, Karnataka-577536, India*
[3]*Centre of Plasma Physics-Institute for Plasma Research, Sonapur, Assam-782402, India*

[*]Corresponding Author: sumatoijam1@gmail.com

(Received 15 September 2025; revised 17 November 2025; accepted 23 November 2025; published 6 April 2026)

Abstract: Polyvinyl alcohol/Polyvinyl pyrrolidone/Zinc oxide (PVA/PVP/ZnO) polymer blend nanocomposites has been prepared to explore their optical and transport properties. The prepared sample are characterized by X-ray diffraction, Atomic force microscope, Energy-dispersive X-ray analysis, UV-visible spectroscopy and Fourier transform infra-red for structural, morphological, elemental and optical properties. The gradual reduction in the optical band gap energy from 5.30 eV to 2.10 eV is observed when the ZnO content in the PVA/PVP blend matrix increases. The nanocomposites also exhibit negligible transmittance in the UV region, indicating their potential for UV-shielding applications. The dielectric constant values of these nanocomposites are found in the range 14-23 with dielectric loss value of 0.06. The conduction mechanism observed in AC conductivity for all samples is governed by small polaron tunnelling model (SPTM). These results suggest that PVA/PVP/ZnO nanocomposites are suitable candidates for use as an insulator in the development of microelectronic device applications.

Keywords: Polymer blend, Optical properties, dielectric constant, dielectric loss, AC conductivity

PACS: 78.67.Sc, 77.84.Jd, 72.80.Le, 82.35.Np

1 Introduction

Polymer characteristics can be enhanced by blending two or more polymers and incorporating inorganic nanoparticles (NPs) as fillers, enabling their application in areas such as biomedical, thermal conductor, optoelectronics, and electrical insulation [1, 2]. Hydrophilic polymer blends, particularly PVA and PVP, are widely explored for fabricating functional polymer nanocomposites due to their miscible nature. This strong miscibility originates from hydrogen bond formation between the -OH groups of PVA and the C=O groups of PVP. These functional groups effectively interact with various nanofillers, resulting in the development of polymer nanocomposites (PNCs) and complexes with enhanced properties. Such materials are highly desirable for fabricating both current and future biodegradable optoelectronic, microelectronic, and energy storage devices [3, 4]. To optimize the desired thermophysical, dielectric, and electrical properties in flexible nanodielectric polymer matrices, ZnO NPs is often used as filler in the formation of polymer blend nanocomposites (NCs) due to its wide bandgap energy (3.3 eV) and large exciton binding energy (60 meV) [5]. ZnO has been widely utilised in various applications including luminescent and lasing devices, transparent conducting electrodes, ultraviolet blockers, photocatalysts, thin-film transistors, and light-emitting devices [6, 7]. S. H. Zyoud et al. [8] studied on the dielectric and optical parameters of the PVA/PVP/ZnO blend nanocomposite films with different concentration of ZnO (0-5.5 wt%). The results showed that these materials are promising potential in electronic devices and nonlinear optics. S. Jambaladinni et al. [9] investigated the role of ZnO nanofillers (0-15 wt%) on the optical and frequency dependent dielectric and dc conductivity properties of PVA/PVP/ZnO blend polymer, favouring the nanocomposite for potential application in

electromagnetic-induction (EMI). In the present work, optical, dielectric and AC conductivity characteristics of PVA/PVP blend based PNC films with higher loading percentages of ZnO (0, 5, 10, 15 and 20 wt%) has been studied which have been scarcely explored in earlier reports to evaluate their potential in optoelectronic and electronic device applications.

PVA/PVP/ZnO NCs containing varying concentrations of ZnO nanoparticles were synthesized using a simple and economical solution casting method. X-ray diffraction (XRD), Atomic force microscope (AFM), Energy dispersive X-ray analysis (EDX) and UV-visible spectroscopy (UV-Vis) are used to characterize the structural, morphological, elemental composition and optical behaviour of the nanocomposites. Dielectric response and AC conductivity of the samples were examined over a temperature range of 303K-393K and frequency range of 100Hz-1MHz.

2 Experimental

2.1 Materials required

Zinc nitrate tetrahydrate $(\mathrm{Zn(NO_3)_2 \cdot 4H_2O})$, sodium hydroxide (NaOH) procured from MERCK are used as precursor and precipitating agent respectively. Polyvinyl alcohol (PVA) and polyvinyl pyrrolidone (PVP) obtained from Sigma Aldrich are used as polymer for the preparation of NCs. Distilled water is employed as the solvent throughout the synthesis procedure.

2.2 Preparation of PVA/PVP/ZnO nanocomposites (PPZ NCs)

ZnO nanoparticles used in this work were synthesized as reported in our previous study [10]. PVA/PVP/ZnO NCs with different ZnO nanoparticle loadings were obtained through solution casting method. In a typical process, 3g of PVA and 3g of PVP were dissolved in 100ml of distilled water under continuously stirring until clear solution were obtained. The two polymer solutions were then combined and stirred for 2hr to form a homogenous blend. This mixture was divided into five equal portions, after which ZnO nanoparticles were incorporated at concentrations 0, 5, 10, 15 and 20 wt% respectively. Each suspension was ultrasonicated for 1hr and further stirred for 24hr to obtain an even dispersion of nanoparticles within the polymer blend matrix. The resulting solutions were placed in Petri dish and dried at 50°C for 5 hr in an oven. The PVA/PVP/ZnO NCs were labelled as PPZ0, PPZ5, PPZ10, PPZ15, and PPZ20 representing the pure PVA/PVP blend and nanocomposites with 5, 10, 15 and 20 wt% of ZnO NPs content respectively. The films showed an average thickness of approximately $45\mu m \pm 1\mu m$. Fig. 1 depicts the schematic representation of the fabrication procedure.

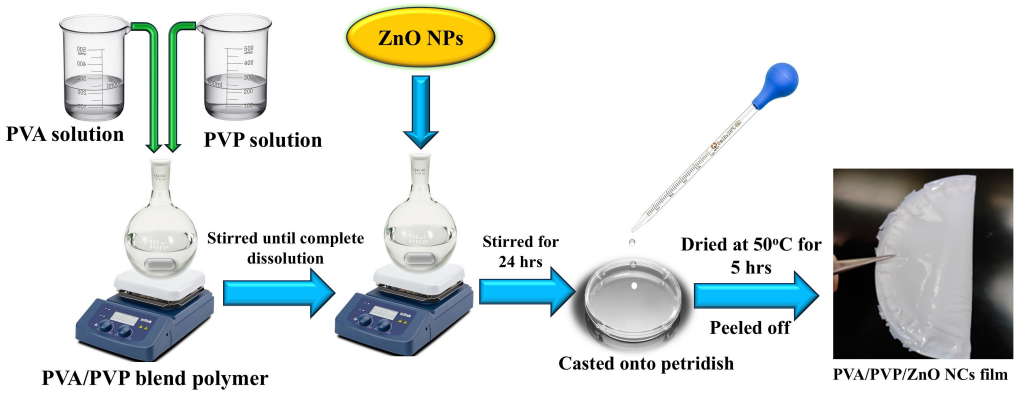

Figure 1: Schematic representation for the preparation of PVA/PVP/ZnO nanocomposites.

3 Characterization

The crystalline structure of the synthesized nanocomposites was analyzed using Phillip's `PANanalytical X'Pert PRO` diffractometer equipped with a Cu target (λ=1.5405Å) operating over a 2θ range of $10° - 80°$. Surface morphology was characterized by atomic force microscope (AFM). Elemental composition was determined

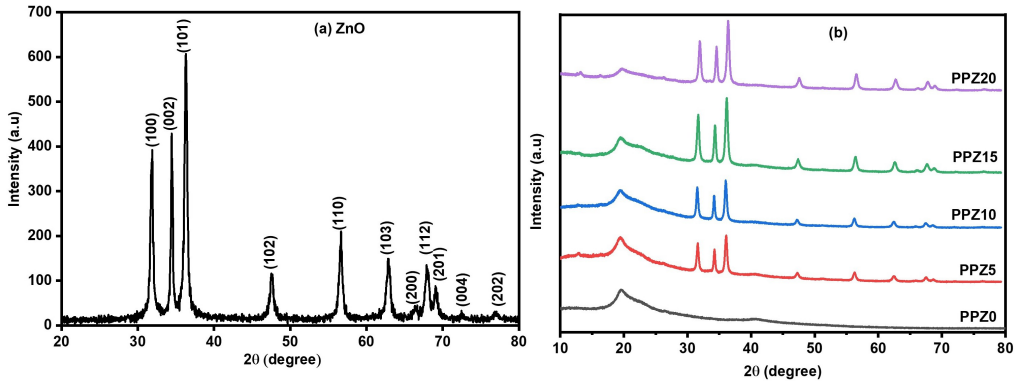

Figure 2: XRD spectra for (a) ZnO NPs and (b) PPZ nanocomposites

using energy dispersive X-ray analysis (EDX) with an `Apollo SDD` detector attached to a SEM `FEI QUANTA 250`. Optical absorption measurement was carried out using UV-visible spectrophotometer (`PerkinElmer Lambda 365`). Fourier transform infra-red (FTIR) spectroscopy analysis was carried out on PerkinElmer Spectrum Two spectrometer over 400cm^{-1} − 4000cm^{-1} while the dielectric response and AC conductivity of the samples were studied from 303K-393K and 100Hz-1MHz using `Agilent 4284A` LCR meter.

4 Results and discussion

4.1 X-ray diffraction (XRD) study

Fig. 2(a) and (b) shows the XRD spectra for ZnO NPs and PPZ NCs with various concentration of ZnO nanoparticles. Crystallite size of ZnO NPs calculated using the Scherrer formula was 20 nm [11]. In PVA/PVP blend NCs, the presence of two broad and intense peaks observed at angles $2\theta = 19.57°$ and $40.43°$ is attributed to the presence of PVA molecules [12] while the PVP exhibits two diffused halos peaks at angles $2\theta = 12.87°$ and $21.80°$ confirming its amorphous structure [13]. Upon incorporation of ZnO nanoparticles into the polymer blend matrix, characteristics ZnO diffraction peaks appear together with those of PVA and PVP. The enhancement of ZnO peak intensities as the filler concentration rises indicates the successful formation of PVA/PVP/ZnO nanocomposites.

4.2 Atomic force microscope (AFM) analysis

Fig. 3 shows the 2D and 3D AFM surface topographical images of PPZ NCs. The corresponding surface roughness values of the nanocomposites expressed as arithmetic mean roughness Ra and the root mean square roughness Rrms determine through AFM analysis using `Gwyddion` software are summarised in Table 1. It is observed from the Table 1, that the surface roughness of the PPZ0 increases with the increase in concentration of ZnO nanoparticles. This rise in surface roughness serves as evidence that ZnO has been effectively incorporated into PPZ0 but also confirms the presence of some agglomeration among the dispersed nanofillers in the blend matrix.

Table 1: Surface topography values for the PVA/PVP/ZnO NCs films

Samples	R_a (nm)	R_{rms} (nm)
PPZ0	1.51	2.01
PPZ5	2.83	3.98
PPZ15	3.99	5.35
PPZ20	4.81	6.14

4.3 Energy dispersive X-ray (EDX) analysis

The EDX spectra for PPZ NCs are presented in Fig. 4(a-e). The PPZ0 sample present only carbon (C) and oxygen (O) as the constituent element whereas PPZ NCs observed the presence of Zn in addition to carbon and oxygen

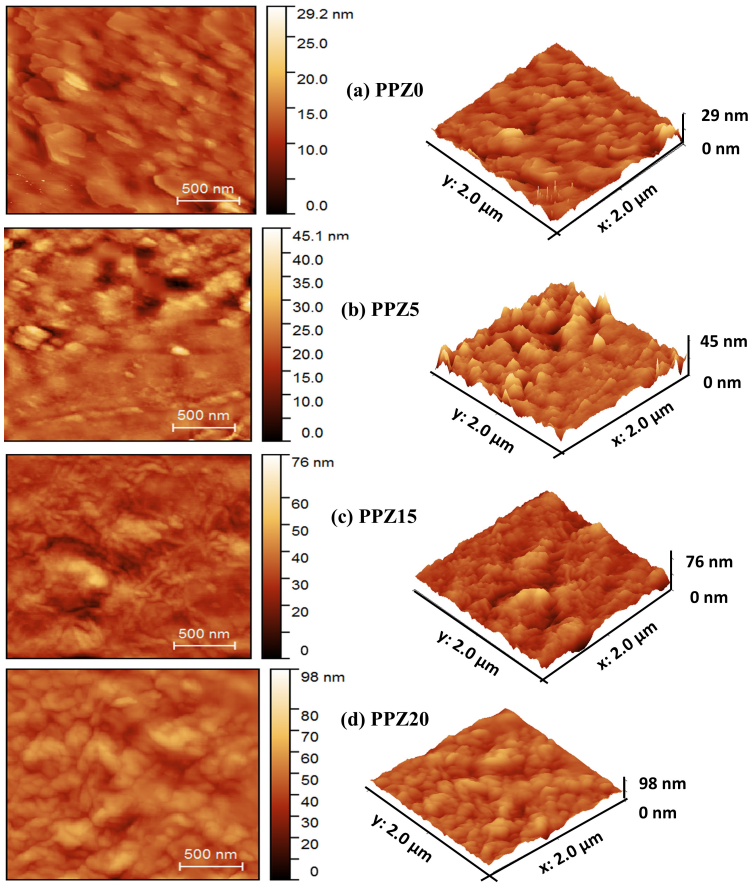

Figure 3: 2D (left side) and 3D (right side) AFM images for PPZ NCs: (a) PPZ0, (b) PPZ5, (c) PPZ15, (d) PPZ20

confirming the successful incorporation of ZnO into the polymer blend matrix. The appearance of two peaks corresponding to Zn in the EDX spectrum arises from the characteristic X-ray emission lines of zinc. The peak observed around 1.02 keV corresponds to the $L\alpha$ emission lines of Zn, while the peaks observed approximately at 8.63 keV are associated with the $K\alpha$ emission lines of Zn.

4.4 UV-visible absorbance spectra

Fig. 5 presented the UV-Vis absorbance spectra for PPZ nanocomposites. The PPZ NCs showed the absorption within the wavelength range of 225-454 nm. With increasing ZnO NPs content in the PVA/PVP blend matrix, an absorption peaks shift toward longer wavelength with varying absorption intensities. In the UV region of the PPZ NCs, there is noticeable light scattering which might be attributed to the increased surface roughness as also evident from the AFM images.

The optical band gap energy is determined using the Tauc's equation (1) from the absorbance spectra

$$(\alpha h\nu)^n = \beta(h\nu - E_g) \tag{1}$$

where α denotes the absorption co-efficient, $h\nu$ represents the photon energy, E_g correspond to the band gap energy, β is the proportionality constant. The exponent n is determined by the nature of the electronic transition with a value of $\frac{1}{2}$ for direct allowed transition and 2 for indirect allowed transition.

The optical band gap energy for direct allowed transition for each sample determined by extrapolating the linear portion of the $(\alpha h\nu)^2$ versus $(h\nu)$ curve to its interaction with the photon energy axis as shown in Fig. 6. From the Tauc's plot, the direct band gap energy for PPZ0, PPZ5, PPZ10, PPZ15 and PPZ20 are 5.30eV, 2.66eV, 2.39eV, 2.19eV and 2.10eV respectively. The introduction of ZnO nanoparticles into the PVA/PVP matrix induces a decrease in band gap energy. This reduction is attributed to the formation of structural defects in the polymer blend matrix caused by the presence of ZnO [14, 15]. The structural defect produces localized state

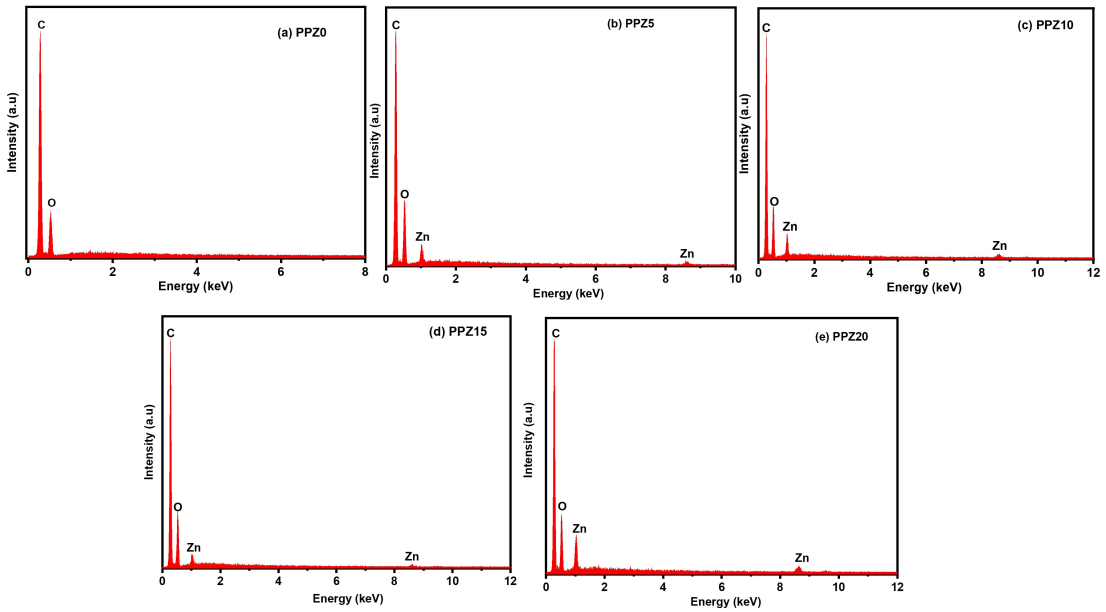

Figure 4: EDX spectra for PPZ NCs: (a) PPZ0, (b) PPZ5, (c) PPZ10, (d) PPZ15, (e) PPZ20

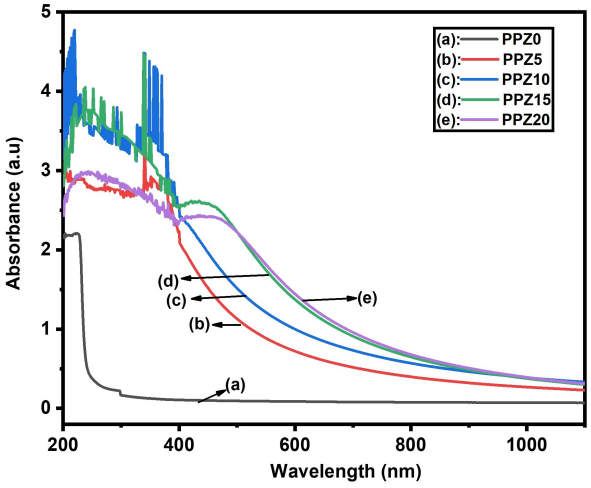

Figure 5: UV-visible absorbance spectra for PPZ nanocomposites: (a) PPZ0, (b) PPZ5, (c) PPZ10, (d) PPZ15 and (e) PPZ20

between highest occupied molecular orbital (HOMO) and the lowest unoccupied molecular orbital (LUMO) of the polymers. As the concentration of ZnO rises within the polymer blend matrix, the number of localized states also increases. These localized states create opportunities for electrons to transition from the valence band to these localized states, or from the localized states to the conduction band, all at energy levels lower than the material's band gap energy. This interplay gives rise to the absorption or emission of photons with energies lower than the band gap energy, effectively causing a reduction in the material's optical band gap [16, 17].

4.5 UV-visible transmittance spectra

Fig. 7 illustrates the UV-visible transmittance spectra of PPZ NCs recorded over the wavelength range of 200 nm-1100nm. As the loading of ZnO nanoparticles within the PVA/PVP blend increases, a gradual decline in transmittance is observed in the visible region, while the ultraviolet region exhibits nearly complete absorption. The

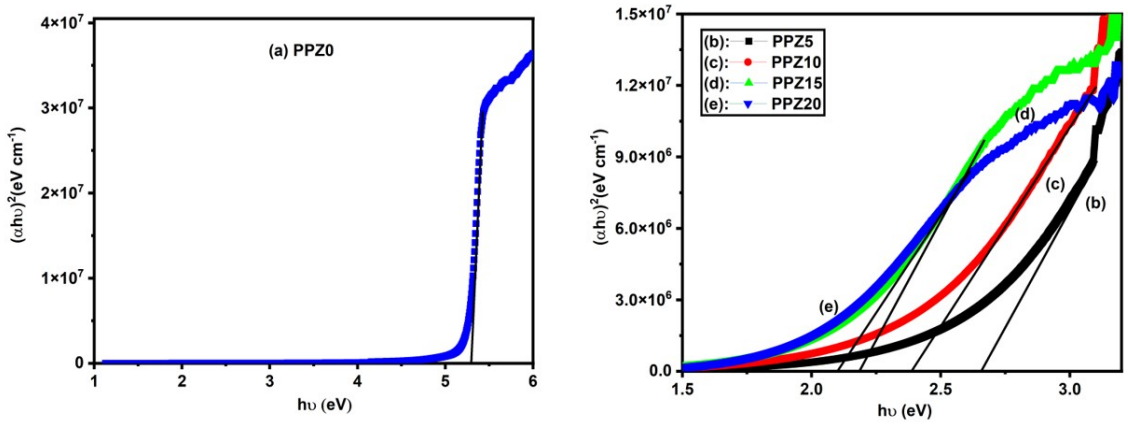

Figure 6: Tauc's plot of $[(\alpha h\nu)^2$ vs. $(h\nu)]$ for PPZ NCs: (a) PPZ0 and (b) PPZ5, PPZ10, PPZ15, PPZ20 NCs.

negligible UV transmittance can be explained by the strong absorption of short-wavelength radiation by electrons in the outer energy levels of ZnO nanoparticles, which become excited to higher energy states and consequently prevent a portion of the incident radiation from passing through the material. Conversely, the pure PVA/PVP polymer blend contains no free charge carriers or intermediate energy states between the HOMO and LUMO levels, and therefore requires photons of higher energy for electronic excitation, resulting in higher transparency. These results demonstrate that the synthesized PPZ NCs possess strong UV-shielding characteristics, making them suitable for UV-protective applications [15, 18].

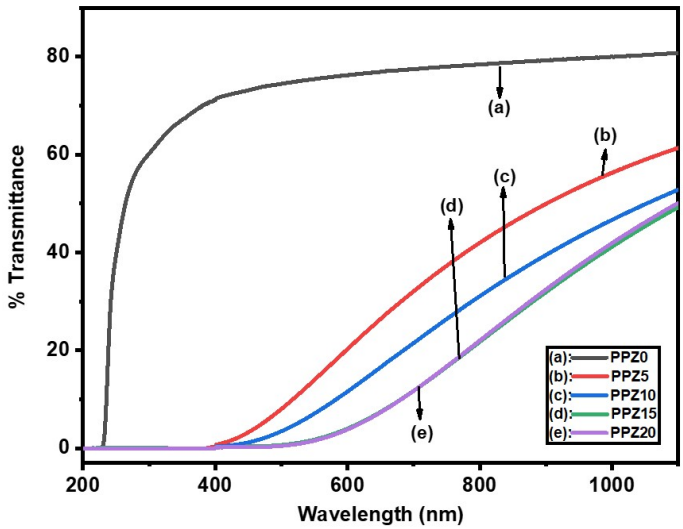

Figure 7: UV-visible transmittance spectra for PPZ nanocomposites: (a) PPZ0, (b) PPZ5, (c) PPZ10, (d) PPZ15, (e) PPZ20

4.6 Fourier transform infra-red analysis

Fig. 8 shows the FTIR spectra for PPZ nanocomposites. A broad and intense absorption band appeared in all samples in the range of 3000 cm^{-1}-3600 cm^{-1} is attributed to the stretching vibration of hydroxyl group (-OH) and slight shifted towards the higher wavenumber with the increasing ZnO nanoparticles content. A band at 2941 cm^{-1} corresponds to the -CH stretching vibration of PVA and PVP. The C=O stretching mode is ascribed at 1658 cm^{-1}. The combination band of (CH+CC) group is identified at 1245 cm^{-1}. The band at 1283 cm^{-1} is attributed to C-N bending vibration. The stretching mode of C-C group are seen at 917cm^{-1} and 852cm^{-1}. The band at 570cm^{-1} is assigned to N-C=O bending vibration. The band at 1080cm^{-1}- arises from the stretching vibration of

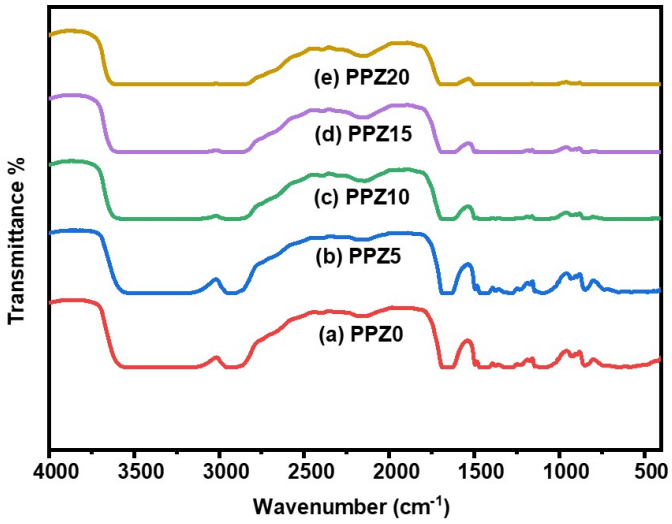

Figure 8: FTIR spectra for PPZ nanocomposites: (a) PPZ0, (b): PPZ5, (c) PPZ10, (d) PPZ15, (e):PPZ20

C-O groups of PVA and a strong band at 1658cm^{-1} is attributed to the C=O stretching vibration of PVP. All the characteristic absorption band observed in the nanocomposites are agrees well with the previous reports [19–21]. As the concentration of ZnO nanoparticles increase, the intensities of some bands are decreased, becomes wider as well as slightly shifted to longer wavelength. This indicates the strong interfacial interaction between the ZnO and miscible chain structure of PVA/PVP.

5 Dielectric properties

5.1 Dielectric constant

For each sample the dielectric constant is evaluated using the expression, $\epsilon = \frac{Cd}{\epsilon_0 A}$, where C denotes the capacitance, d signifies film thickness, A represent film area, ϵ_0 is the permittivity of free space. Fig. 9 depicts the dependence of dielectric constant on frequency at various temperature and variation of dielectric constant with temperature at fixed frequency (inset) for PPZ NCs. The dielectric permittivity of all samples exhibits high values in the low frequency region and gradually declines as the frequency increases. The low frequency response is predominantly controlled by the interfacial polarization commonly referred to as Maxwell-Wagner-Sillars (MWS) mechanism, which is the characteristic feature of polymer-based nanocomposite. In the present samples, semiconducting fillers dispersed within the PVA/PVP polymer blend promotes the charge build up at the filler-polymer interfaces. Variations in charge distribution across these interfaces lead to the formation of large number of micro-capacitors like regions throughout the material which effectively behave as dipoles [10, 22, 23]. At low frequencies, these dipoles can easily orient in response to the applied electric field, resulting in strong polarization and high dielectric permittivity. With increasing frequency, dipole orientation becomes progressively hindered, leading to a decrease in the dielectric constant.

In addition, it can be observed that the dielectric constant of all samples rises with the increasing temperature at a given frequency. At lower temperature, the polymer films exhibit smaller dielectric constant values because limited thermal energy restricts dipole motion, rendering the dipoles associated with the micro-capacitive regions and the polar PVA/PVP matrix relatively immobile and less responsive to the applied electric field. As the temperature increases, the flexibility of polymer chain, polar functional groups and dipolar species within the system improves. This increased molecular mobility shortens the relaxation time of both polymer segments and dipoles, allowing them to respond more readily to variations in the external electric field. As a result, an enhancement in dielectric constant is observed [15, 24, 25]. Fig. 9(f) shows the variation of dielectric constant with frequency for different concentration of ZnO nanoparticles at 393K. From the graph, it is observed that the dielectric constant value of PPZ0, PPZ5, PPZ10, PPZ15 and PPZ20 does not vary much with values of 14, 15, 13, 16 and 23 respectively. Such PPZ NCs which has lower dielectric constant value suggests their suitability for use as an insulator in the fabrication of micro electronic device applications.

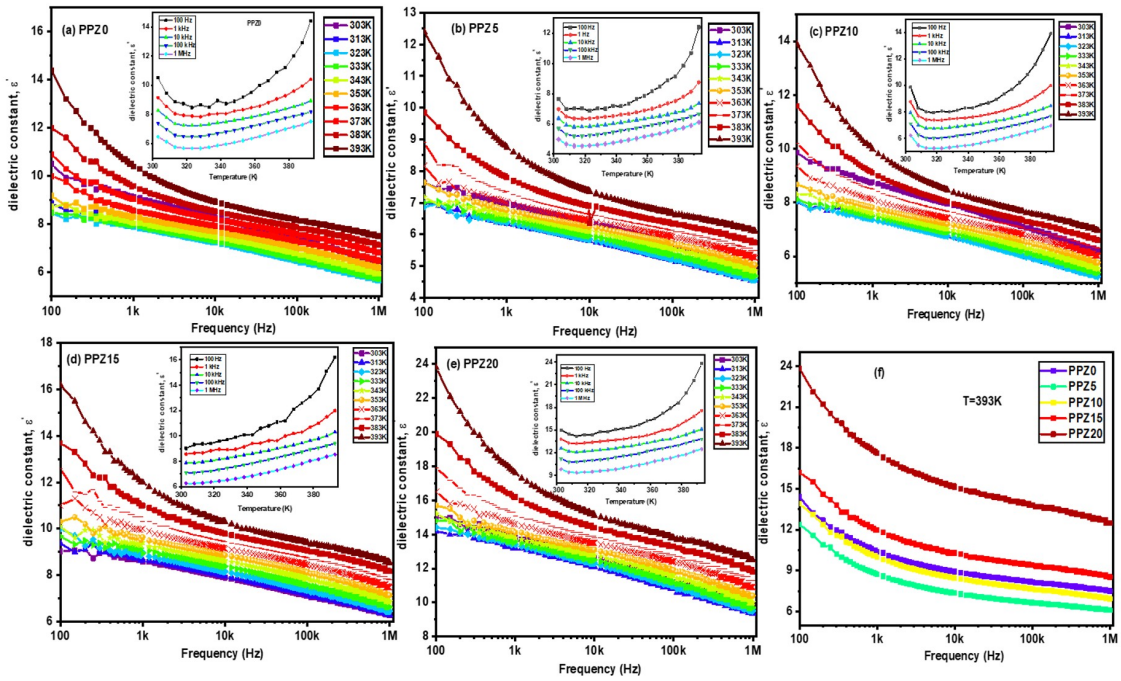

Figure 9: Frequency variation of dielectric constant at different temperatures and temperature-dependent dielectric constant (inset) at a fixed frequency for PPZ nanocomposites: (a) PPZ0, (b) PPZ5, (c)PPZ10, (d) PPZ15, (e) PPZ20 and (f) frequency-dependent dielectric behaviour for different PPZ NC loadings.

5.2 Dielectric loss

Fig. 10(a-e) illustrate the frequency-dependent dielectric loss of PPZ nanocomposites measured at different temperature, along with the temperature variation of dielectric loss at a chosen frequency shown in inset graph. The samples exhibit relatively high dielectric loss in the low-frequency region, which is mainly attributed to interfacial polarization effect. As the frequency increases, the dipoles are unable to keep pace with the rapid oscillations of the applied electric field, leading to a gradual reduction in the dielectric loss. The inset plot further reveals that dielectric loss increases with the increasing temperature. This behaviour can be explained by the formation of additional free volume within the polymer blend matrix at elevated temperature, which facilitates dipolar reorientation and thereby enhances dielectric loss [26–29]. Moreover, the dielectric loss values decrease from approximately 0.9 at low frequencies to about 0.06 at frequencies above 100 kHz for all samples, as shown in Fig. 10(f). The observed low dielectric loss at higher frequencies indicates that these nanocomposites are promising candidates for low-loss dielectric applications.

5.3 AC Conductivity

The AC conductivity for each sample is evaluated using Eq. (2) by utilizing the dielectric constant and dielectric loss data derived from dielectric measurements over the temperature range of 303K-393 K and the frequency range of 100Hz -1MHz to further understand the electrical conduction mechanism.

$$\sigma_{ac} = 2\pi f \epsilon \epsilon_0 \tan\delta \tag{2}$$

Here, f represents the frequency of the applied electric field, ϵ_0 denotes the permittivity of free space, ϵ corresponds to the dielectric constant, and $\tan\delta$ refers to the dielectric loss tangent.

Fig. 11(a-e) displays AC conductivity varies with frequency for all samples at specific temperature. It is observed from the graph that the AC conductivity for all the samples shows a linear behaviour upto a frequency of 10kHz and then increased non-linearly at higher frequency. The linear response in the low frequency region indicates that charge transport is dominated by the localized motion of charge carrier associated with interfacial polarization arising from Maxwell-Wagner-Sillars effect. Whereas the non-linear dispersion at higher frequency over the frequency range 10kHz to 1MHz is attributed to the motion of localized charge carrier over the shorter

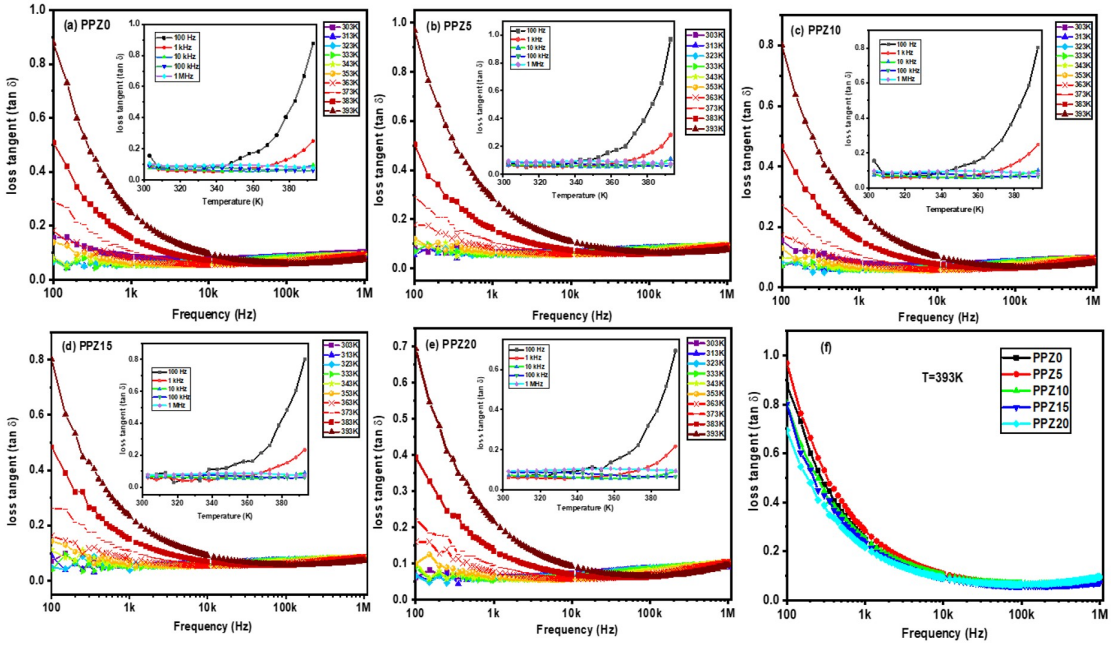

Figure 10: Frequency variation of dielectric loss at various temperature and temperature dependent dielectric loss at a fixed frequency for PPZ nanocomposites: (a) PPZ0, (b) PPZ5, (c) PPZ10, (d) PPZ15, (e) PPZ20 and (f) Frequency dependent dielectric loss for PPZ NCs.

path. The AC conductivity values for all samples at 100Hz for 313K are around 10^{-9}(S/m) and at 393K are around 10^{-7}(S/m). The values of AC conductivity increase with the increase in frequency and found to be 10^{-5}(S/m) at 1MHz. Such low conductivity value indicates that these NCs are promising materials for use as flexible dielectric substrates and insulating layers in biodegradable electronic devices. The conductivity data is evaluated using the

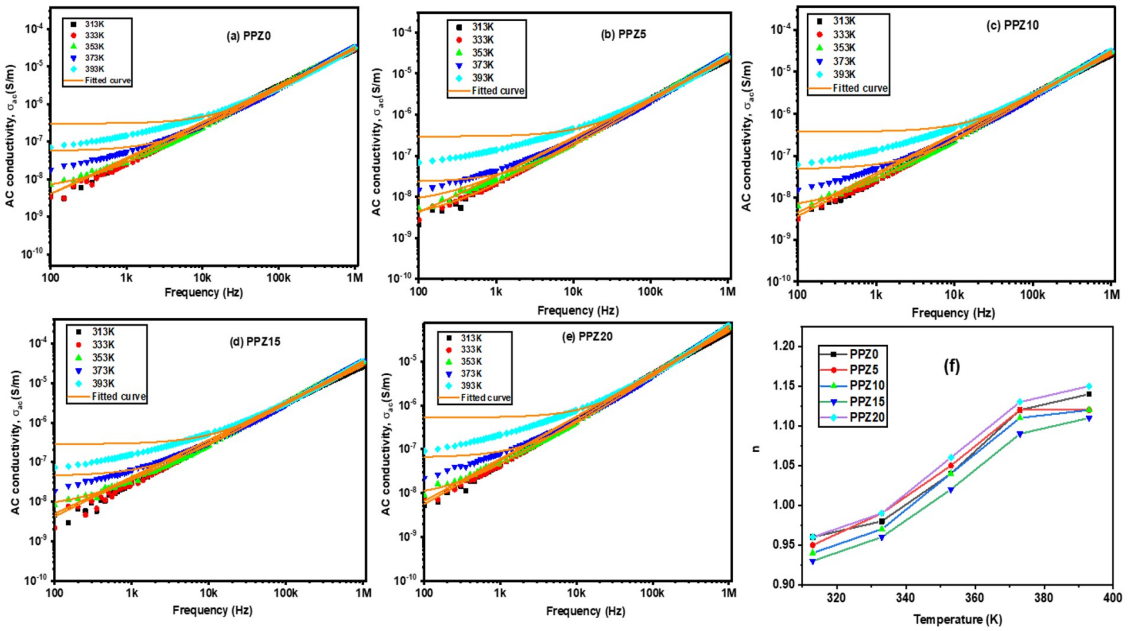

Figure 11: Frequency variation of AC conductivity for PPZ nanocomposites at selected temperature: (a) PPZ0 (b) PPZ5 (c) PPZ10 (d) PPZ15 (e)PPZ20 and (f) Variation of the fit parameter 'n' with temperature.

Jonscher's power law relation expressed as, $\sigma(f) = \sigma_0 + Af^n$. In this relation $\sigma(f)$ denotes the total conductivity, σ_0 represents the dc component of the conductivity, A is the constant related to the strength of the polarizability and n is the frequency exponent that describes the extent of interaction between charge carriers and the lattice. Several theoretical models have been proposed to describe charge transport based on the behavior of n, including the Quantum Mechanical Tunnelling (QMT) model, where n depends on frequency but remains independent of temperature; the Correlated Barrier Hopping (CBH) model, in which n decreases with increasing temperature; the Small Polaron Tunnelling (SPT) model, where n increases with temperature; and the Large Polaron Quantum Mechanical Tunnelling (LPQMT) model, in which n initially decreases to a minimum and then increases as temperature rises. As shown in Fig. 11(f), the value of n increases with temperature, indicating that charge transport in PPZ NCs follows the small polaron tunnelling mechanism [30].

6 Conclusion

PVA/PVP/ZnO nanocomposites containing different ZnO loadings (0, 5, 10, 15, and 20wt%) were synthesized using the solution casting technique. The formation of polymer nanocomposites and the purity of the samples were confirmed through XRD and EDX analyses. AFM images indicate that incorporating ZnO nanoparticles leads to an increase in surface roughness. The band gap energy of the nanocomposites decreases with the increasing concentration of ZnO from 5.30eV to 2.10eV. UV-visible transmittance studies revealed a decrease in transmittance with increasing ZnO concentration, effectively blocking UV radiation, rendering them suitable for UV-shielding applications. FTIR results demonstrate physical interactions between ZnO nanoparticles and the hydroxyl groups of PVA as well as the carbonyl groups of PVP. The dielectric constant values at 393K for PPZ0, PPZ5, PPZ10, PPZ15, and PPZ20 are 14, 15, 13, 16, and 23 respectively. The value of dielectric loss for all samples at lower frequency is of the order of around 0.9 which reduces to 0.06 at higher frequency (above 100 kHz). The values of AC conductivity increase with the increase in frequency and found to be 10^{-5}(S/m) at 1MHz. The frequency-dependent conductivity behaviour follows Jonscher's power law, and the dominant conduction process is attributed to the small polaron tunnelling model. The combination of low dielectric constant, low dielectric loss, and AC conductivity suggests that these nanocomposites are promising candidates as flexible nanodielectric substrates and insulating materials for microelectronic device fabrication.

References

[1] S. Mallakpour and M. Khani, Colloid and Polymer Science **294**, 583 (2016).

[2] D. Rithesh Raj, S. Prasanth, T. Vineeshkumar, and C. Sudarsanakumar, Optics Communications **340**, 86 (2015).

[3] K. Rajesh, V. Crasta, N. B. Rithin Kumar, G. Shetty, and P. D. Rekha, Journal of Polymer Research **26**, 99 (2019).

[4] P. Dhatarwal and R. J. Sengwa, Advanced Composites and Hybrid Materials **3**, 344 (2020).

[5] S. Shinde, P. Shinde, Y. Oh, D. Haranath, C. Bhosale, and K. Rajpure, Applied Surface Science **258**, 9969 (2012).

[6] H. Kim, C. M. Gilmore, J. S. Horwitz, A. Piqué, H. Murata, G. P. Kushto, R. Schlaf, Z. H. Kafafi, and D. B. Chrisey, Applied Physics Letters **76**, 259 (2000).

[7] Özgür, Y. I. Alivov, C. Liu, A. Teke, M. A. Reshchikov, S. Doğan, V. Avrutin, S.-J. Cho, and H. Morkoç, Journal of Applied Physics **98**, 041301 (2005).

[8] S. H. Zyoud, T. H. AlAbdulaal, A. Almoadi, M. S. Alqahtani, F. A. Harraz, M. S. Al-Assiri, I. S. Yahia, H. Y. Zahran, M. I. Mohammed, and M. S. Abdel-wahab, Crystals **13** (2023).

[9] S. Jambaladinni and J. S. Bhat, Iranian Journal of Science and Technology, Transactions A: Science **45**, 1851 (2021).

[10] T. S. Chanu, K. J. Singh, W. J. Singh, and K. N. Devi, Physica Status Solidi (A) **220**, 2300531.

[11] T. Suma Chanu, K. Jugeshwar Singh, and K. Nomita Devi, Materials Today: Proceedings **65**, 2844 (2022).

[12] P. L. Reddy, K. Deshmukh, K. Chidambaram, M. M. N. Ali, K. K. Sadasivuni, Y. R. Kumar, R. Lakshmipathy, and S. K. K. Pasha, Journal of Materials Science: Materials in Electronics **30**, 4676 (2019).

[13] P. Dhatarwal, S. Choudhary, and R. Sengwa, Materials Letters **273**, 127913 (2020).

[14] J. Rozra, I. Saini, A. Sharma, N. Chandak, S. Aggarwal, R. Dhiman, and P. K. Sharma, Materials Chemistry and Physics **134**, 1121 (2012).

[15] T. S. Chanu, K. J. Singh, and K. N. Devi, Polymer Bulletin **81**, 5069 (2024).

[16] K. Hemalatha, K. Rukmani, N. Suriyamurthy, and B. Nagabhushana, Materials Research Bulletin **51**, 438 (2014).

[17] J. Rozra, I. Saini, A. Sharma, N. Chandak, S. Aggarwal, R. Dhiman, and P. K. Sharma, Materials Chemistry and Physics **134**, 1121 (2012).

[18] H. S. Roy, M. Y. A. Mollah, M. M. Islam, and M. A. B. H. Susan, Polymer Bulletin **75**, 5629 (2018).

[19] C. L. Raju, J. L. Rao, B. C. V. Reddy, and K. Veera Brahmam, Bulletin of Materials Science **30**, 215 (2007).

[20] M. M. Rahman Khan, S. Pal, M. M. Hoque, M. R. Alam, M. Younus, and H. Kobayashi, ACS Omega **4**, 6144 (2019).

[21] E. M. Abdelrazek, A. M. Abdelghany, A. E. Tarabiah, and H. M. Zidan, Journal of Materials Science: Materials in Electronics **30**, 15521 (2019).

[22] K. S. Hemalatha, G. Sriprakash, M. V. N. Ambika Prasad, R. Damle, and K. Rukmani, Journal of Applied Physics **118**, 154103 (2015).

[23] R. C. Smith, C. Liang, M. Landry, J. K. Nelson, and L. S. Schadler, IEEE Transactions on Dielectrics and Electrical Insulation **15**, 187 (2008).

[24] A. H. Mohamad, O. G. Abdullah, and S. R. Saeed, Results in Physics **16**, 102898 (2020).

[25] B. M. Baraker and B. Lobo, Bulletin of Materials Science **42**, 18 (2019).

[26] M. S. Gaur, A. P. Indolia, A. A. Rogachev, and A. V. Rahachou, Journal of Thermal Analysis and Calorimetry **122**, 1403 (2015).

[27] P. Mukherjee, A. Das, B. Dutta, and A. Meikap, Journal of Physics and Chemistry of Solids **111**, 266 (2017).

[28] R. J. Sengwa, S. Choudhary, and P. Dhatarwal, Advanced Composites and Hybrid Materials **2**, 162 (2019).

[29] S. Choudhary, Polymer Composites **39**, E1788.

[30] M. Dult, R. Kundu, J. Hooda, S. Murugavel, R. Punia, and N. Kishore, Journal of Non-Crystalline Solids **423-424**, 1 (2015).